The 8th International Conference on Jets, Wakes and Separated Flows, ICJWSF-2024
September 23-25, 2024, Firenze, Italy

Modelling Leading Edge Erosion of Wind Turbine Blades

C. Holzinger[1] and B. Semlitsch[1*]

1: Institute of Energy Systems and Thermodynamics, TU Wien, Austria

[*] Corresponding author: bernhard.semlitsch@tuwien.ac.at

Abstract

Wind turbines have substantially contributed to sustainable energy transitions over the last two decades, harvesting renewable energy. The installed wind turbine rotor blades are exposed to all weather conditions throughout their lifetime, wearing down the surfaces, especially the leading edges. The increased surface roughness amplifies the drag forces and, hence, decreases the aerodynamic performance. Forecasting models are needed to evaluate the economic benefit of repair realistically for certain erosion states of wind turbine blades. Although numerous methodologies exist for loss prediction due to surface roughness, the development and validation of such models are needed. Therefore, we establish numerical flow simulation methodologies to predict torque losses for eroded (below mesh resolution) and severely damaged (of the order of the mesh resolution) wind turbine wings. While severe damages, such as delamination, can be described by the computational mesh, the required roughness representation at the subgrid scale is performed using the amplification roughness model. Being an extension of the Langtry-Menter γ-$Re_{\theta t}$ turbulence model, the amplification roughness model can handle the transition prediction between laminar and turbulent flow regimes even for rough surfaces. The reliability of the suggested methodologies is validated by two-dimensional test cases from literature for representative airfoils and erosion states.

Keyword: *Wind energy, Surface erosion, Flow separation, Numerical flow simulation, Turbulence modelling*

1. Introduction

Wind turbines have become, over the last two decades, a substantial contributor to harvesting renewable energy [2]. The installed turbines have been exposed to different weather conditions throughout their lifetime. Raindrops, hail, ice, airborne particles, and insects impact the rotor blades of the wind turbine and degrade their surfaces [6, 10], which manifests mostly at the leading edge and blade outermost regions. Leading edge erosion reduces the aerodynamic performance, and hence the annual electricity production by up to 10% [4, 3]. Moreover, the increased surface roughness can cause larger flow structure generation and amplify thereby the vibrational load. Thus, maintenance is required after certain periods of operation but shall be only performed in economically beneficial scenarios.

Erosion damage on wind turbines starts with increasing roughness manifesting as pits and grows continuously to gouges on the impacted turbine wing surface over exposure time. Finally, delamination of the underlying composite laminates can occur [6, 1]. A rougher surface causes flow momentum losses in the boundary layer and early transition to turbulence. Thereby, the drag increases and the lift reduces, especially in the upper part of the drag polar [12], where flow separation might occur due to the steep angle of attack.

The Reynolds-Averaged Navier-Stokes (RANS) equations are commonly simulated to obtain accurate predictions of the flow structures, losses, and separation over wings. Surface roughness can be quantified by the roughness Reynolds number, $Re_r = uk_r/\nu$ in the context of aerodynamics, where u is the local flow velocity, k_r is the roughness height, and ν is the kinematic viscosity. Surfaces can be considered as smooth for values of Re_r below 120, while roughness models are required beyond that threshold value. Such models are commonly based on an equivalent sand grain roughness to mimic the same skin friction losses, which cannot be straightforwardly related to a physical parameter and thus, empirical correlations are required. Castorrini et al. [3] represented the erosion pits in the wind turbine blade geometry and predicted the boundary layer transition using the Langtry-Menter $\gamma - Re_{\theta t}$ turbulence model. Schramm et al. [13]

and Wang et al. [15] analysed the impact of wind turbine blade delamination and pitting by representing the damage in the two-dimensional mesh.

Transition turbulence models are required to capture the subgrid effect of boundary layer transition to turbulence due to surface erosion on the wind turbine performance by efficient computational simulations. The incomplete knowledge of the non-physical parameters challenges this numerical simulation strategy. Hence, validation with experimental data is required to establish correlations between the model parameters and the measured data. We perform numerical flow simulations around two-dimensional airfoils with pitting and delamination damage and validate the results against experimental data. The amplification roughness turbulence model is applied for damages below mesh resolution, i.e. pits and gouges, whereas a geometrically resolved methodology is employed for severely damaged wind turbine blades, i.e. due to delamination.

2. Methodology

Fluid dynamic phenomena, e.g. transition to turbulence, flow separation, and flow momentum losses, of an incompressible behaving medium and constant viscosity on wind turbine airfoils can be predicted by the Navier-Stokes equations;

$$\frac{\partial u_i}{\partial t} + \frac{\partial}{\partial x_j}\left(u_j u_i\right) = -\frac{1}{\varrho}\frac{p}{\partial x_i} + \frac{\partial}{\partial x_j}\left(\nu\left(\frac{\partial u_i}{\partial x_j} + \frac{\partial u_j}{\partial x_i}\right)\right) , \tag{1}$$

and the mass conservation equation,

$$\frac{\partial u_i}{\partial x_i} = 0 , \tag{2}$$

where x are the spatial coordinates, t is the time, u is the flow velocity, ϱ is the density, p is the static pressure, and ν is the kinematic viscosity. Not all flow scales are represented on the numerical mesh to be computationally efficient. To model turbulence, the governing set of equations is Reynold-averaged, where the flow variables are decomposed into a mean $\overline{u}$ and a fluctuation u' component. Per definition, the temporal average of the fluctuating components is zero. Thereby, the Reynold-Averaged Navier-Stokes equations can be written as,

$$\frac{\partial \overline{u}_i}{\partial t} + \overline{u}_j\frac{\partial \overline{u}_i}{\partial x_j} = -\frac{1}{\varrho}\frac{\partial \overline{p}}{\partial x_i} + \nu\frac{\partial^2 \overline{u}_i}{\partial x_j^2} - \frac{\partial \overline{u_i' u_j'}}{\partial x_j} . \tag{3}$$

The additional term, i.e. the Reynolds stress tensor $\overline{u_i' u_j'}$, has to be modelled to close the equation system. Applying the Boussinesq's approximation, the Reynolds stress tensor can be expressed as,

$$\overline{u_i' u_j'} = -\nu_t\left(\frac{\partial \overline{u}_i}{\partial x_j} + \frac{\partial \overline{u}_j}{\partial x_i} - \frac{2}{3}\frac{\partial \overline{u}_k}{\partial x_k}\delta_{ij}\right) + \frac{2}{3}\varrho k\delta_{ij} , \tag{4}$$

where δ_{ij} is the Kronecker delta, ν_t is the kinematic eddy viscosity, and k is the turbulence kinetic energy. Estimates for the kinematic eddy viscosity and the turbulent kinetic energy can be obtained by algebraic models or additional transport equations. The k-ω shear stress transport (SST) turbulence model by Menter [11] utilises two transport equations for the turbulence kinetic energy, k,

$$\frac{\partial k}{\partial t} + \frac{\partial\left(\overline{u}_j k\right)}{\partial x_j} = P_k - \beta^* k\omega + \frac{\partial}{\partial x_j}\left[\left(\nu + \sigma_k \nu_t\right)\frac{\partial k}{\partial x_j}\right] , \tag{5}$$

and the specific turbulence dissipation rate, ω,

$$\frac{\partial \omega}{\partial t} + \frac{\partial\left(\overline{u}_j \omega\right)}{\partial x_j} = \frac{\alpha}{\nu_t}P_k - \beta\omega^2 + \frac{\partial}{\partial x_j}\left[\left(\nu + \sigma_\omega \nu_t\right)\frac{\partial \omega}{\partial x_j}\right] + 2\left(1 - F_1\right)\frac{\sigma_{w2}}{\omega}\frac{\partial k}{\partial x_j}\frac{\partial \omega}{\partial x_j} , \tag{6}$$

where P_k is the turbulent shear stress production term, and β^*, σ_k, α, β, σ_ω and $\sigma_{\omega 2}$ are model coefficients. By blending between the k-ε and the k-ω turbulence models based on the non-slip wall proximity with the function F_1, the advantages of the two models are combined. The kinematic eddy viscosity can be calculated by,

$$\nu_t = \frac{a_1 k}{\max\left(a_1\omega, \Omega F_2\right)} , \tag{7}$$

where a_1 is a model coefficient, Ω is the strain-rate magnitude, and F_2 acts as a limiting function towards the non-slip walls. The k-ω SST turbulence model has been extended by Langtry and Menter [9] to predict turbulent transition. Therefore, the Langtry-Menter γ-$Re_{\theta t}$ turbulence model solves two additional transport equations for the intermittency, γ,

$$\frac{\partial \gamma}{\partial t} + \frac{\partial \left(u_j \gamma\right)}{\partial x_j} = P_\gamma - E_\gamma + \frac{\partial}{\partial x_j}\left[\left(\nu + \frac{\nu_t}{\sigma_f}\right)\frac{\partial \gamma}{\partial x_j}\right], \tag{8}$$

and the local transition onset momentum thickness Reynolds number, $Re_{\theta t}$,

$$\frac{\partial Re_{\theta t}}{\partial t} + \frac{\partial \left(u_j Re_{\theta t}\right)}{\partial x_j} = P_{\theta t} + \frac{\partial}{\partial x_j}\left[\sigma_{\theta t}\left(\nu + \nu_t\right)\frac{\partial Re_{\theta t}}{\partial x_j}\right], \tag{9}$$

where P_γ and $P_{\theta t}$ are the source terms, E_γ is the , and σ_f and $\sigma_{\theta t}$ are model coefficients. The value of $Re_{\theta t}$ is computed based on the free-stream turbulence intensity and a pressure gradient parameter. A trigger function activates the intermittency production when $Re_{\theta t}$ reaches a critical threshold value, Re_θ. The variable γ denotes the state of the boundary layer, i.e. laminar, $\gamma = 0$, and turbulent, $\gamma = 1$. The turbulent shear stress production term and the dissipative terms are scaled with the intermittency. Additionally, the blending function, F_1, is modified such that F_1 cannot reach zero for laminar boundary layers. Langel et al. [8] extended the Langtry-Menter γ-$Re_{\theta t}$ turbulence model to handle surface roughness. The amplification roughness A_r is transported as a passive scalar through the computational domain by solving the equation,

$$\frac{\partial A_r}{\partial t} + \frac{\partial \left(u_j A_r\right)}{\partial x_j} = \frac{\partial}{\partial x_j}\left[\sigma_{Ar}\left(\nu + \nu_t\right)\frac{\partial A_r}{\partial x_j}\right], \tag{10}$$

where σ_{Ar} is a constant. Thereby, not only the wall next cell has information on the surface roughness but also all downstream cells. The values of the amplification roughness A_r are defined as boundary conditions at the non-slip walls,

$$A_{r|wall} = f\left(k_s^+\right) = \frac{C_{Ar1}}{1 + e^{-\left(C_{Ar2}k_s^+ + C_{Ar3}\right)}}, \tag{11}$$

where k_s^+ is correlated to the physical roughness height by a density distribution function, and C_{Ar1}, C_{Ar2} and C_{Ar3} are constants. Further, the source term, $P_{\theta t}$, is modified and boundary conditions for the specific dissipation rate, ω, at the rough non-slip walls are $\omega_{wall|rough} = u_\tau^2 S_r/\nu$, where $S_r = \left(50/k_s^+\right)^2$ in case of $k_s^+ \leq 25$ and $S_r = 100/k_s^+$ in case of $k_s^+ > 25$.

Two airfoil geometries of the NACA six-digit series with sharp trailing edge are investigated, i.e. the NACA 64-618 and the NACA 64_3-618 shown in Fig. 1 (a). Aerodynamic data is available for the NACA 64-618, which is commonly used in wind turbine research. Nevertheless, experimental data with surface damages is only available for the NACA 64_3-618. The computational domain has been discretised using C-type structured meshes, as shown in Fig. 1 (b), with refinements towards the no-slip walls such that $y^+ < 1$. The domain boundaries have been placed at least 20 times the cord length from the airfoil. A free-stream type boundary condition has been specified for the velocity and pressure at all boundaries. The reference

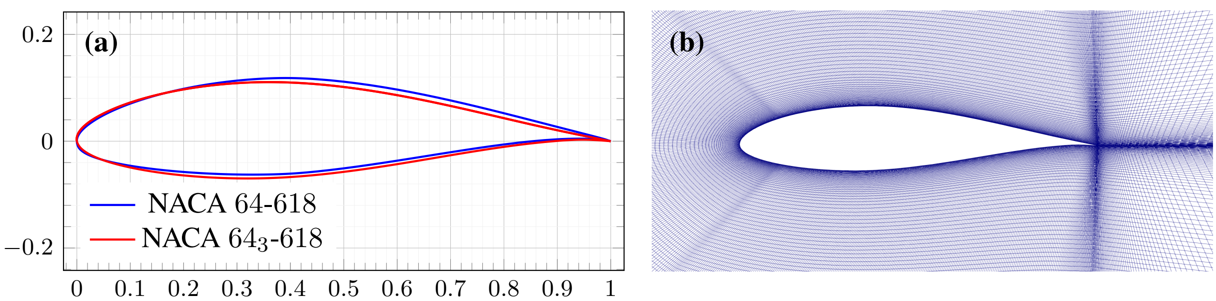

Fig. 1: The contours of the NACA 64-618 and the NACA 64_3-618 are illustrated in subfigure (a). The numerical mesh is shown in subfigure (b).

pressure value was set to zero, and the velocity was set to match a Reynolds number, where the cord length was used as the characteristic length scale. The parameters describing the fluid media have been prescribed to represent air.

The numerical simulations have been performed with the finite volume bases code *OpenFOAM* v1912. The *simple* algorithm has been employed to solve the velocity/pressure coupling for the steady-state computations, where under-relaxation factors of 0.95 have been used. The simulations have been considered as converged when the lift and drag coefficients change less than 10^{-5}. A cell-limited Gauss linear scheme has been used to discretise the gradients. A second-order upwind scheme is used for the divergence of velocity, and a central second-order scheme is used for all other divergence terms.

3. Results

The presented methodology is compared to wind tunnel experiments by Timmer [14] in Fig. 2 in terms of lift and polar curves. The results obtained with both turbulence models, i.e. the k-ω SST and the Langtry-Menter γ-$Re_{\theta t}$ turbulence model, show excellent agreement with the experimental data in the linear regime of lift coefficient vs angle of attack. For high angles of attack where flow separation is expected, the Langtry-Menter γ-$Re_{\theta t}$ turbulence model exhibits clearly benefits over the k-ω SST turbulence model. Hence, laminar to turbulence transition has a significant impact on the prediction of flow separation on the airfoil. Also, the polar curves shown in Fig. 2 (b) reveal good agreement between the numerical predictions and the measurements. Differences in the drag coefficient can be noted at negative angles of attack.

Erosion on wind turbine blades can be categorised into damages causing increased surface roughness (below mesh resolution) and larger delamination damages (representable with the mesh resolution). Because the effects of length scales below mesh resolution require modelling and length scales being resolved by numerical discretisation, different approaches are required to cope effectively with both damage categories.

The amplification roughness model mimics the effect of pits and gouges on the airfoil performance, which cannot be effectively represented on the computational mesh. First, the roughness parameter, k_s, has to be calibrated to describe the physical surface roughness, k_r, which is not straightforward. In the present study, the value $k_r = 100$ μm was modelled as $k_s = 57$ μm and the value $k_r = 200$ μm was modelled as $k_s = 101$ μm to represent the investigated cases by Langel et al. [8]. The NACA 64_3-618 has been considered at a Reynolds number of $3.2 \cdot 10^6$, where surface roughness was applied from the leading edge until 2% of the cord length on the upper surface and 13% of the cord length on the lower surface. The computational predictions have been compared to wind tunnel experiments by Langel et al. [8] and are shown in Fig. 3. Fig. 3 shows that the amplification roughness model can capture the essential trends that occur with increasing surface roughness, but the drag is underestimated.

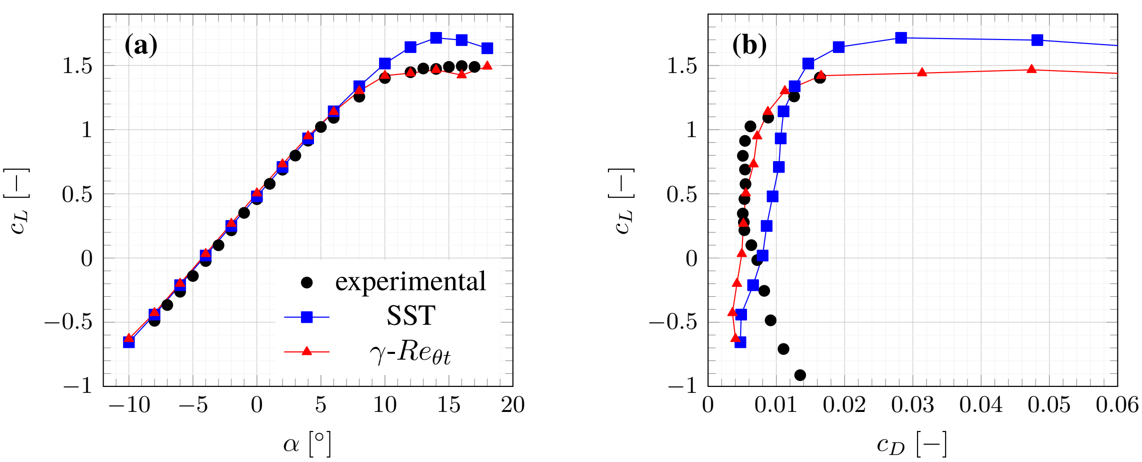

Fig. 2: The numerically estimated lift and polar curves are compared to experimental wind tunnel measurements [14] for a Reynolds number of $6 \cdot 10^6$.

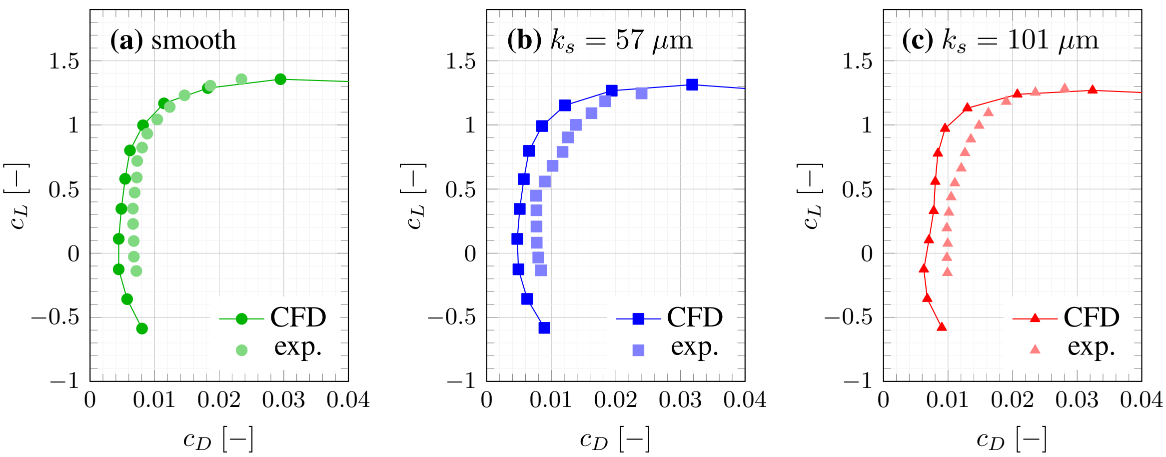

Fig. 3: The polar curves are shown with and without surface roughness on the NACA 64_3-618 geometry, which is compared to experimental data by Langel et al. [8] for a Reynolds number of $3.2 \cdot 10^6$.

The impact of delamination of the size $d = 0.3\%$ and $s = 3\%$ of the cord length on the lift and polar curves is plotted in Fig. 4. The generated lift by the airfoil with and without delamination damage is similar in the linear regime, but the drag is significantly higher with delamination damage. The generated lift drops due to the delamination damage with an angle of attack of $8°$ and remains clearly below the lift achieved with smooth airfoils. The comparison of the numerical predictions with the experimental measurements shows a good agreement. The drag is slightly underestimated for the smooth airfoil as compared to the experiments, while the lift is predicted to be too low for the delamination cases at high angles of attack where flow separation occurred.

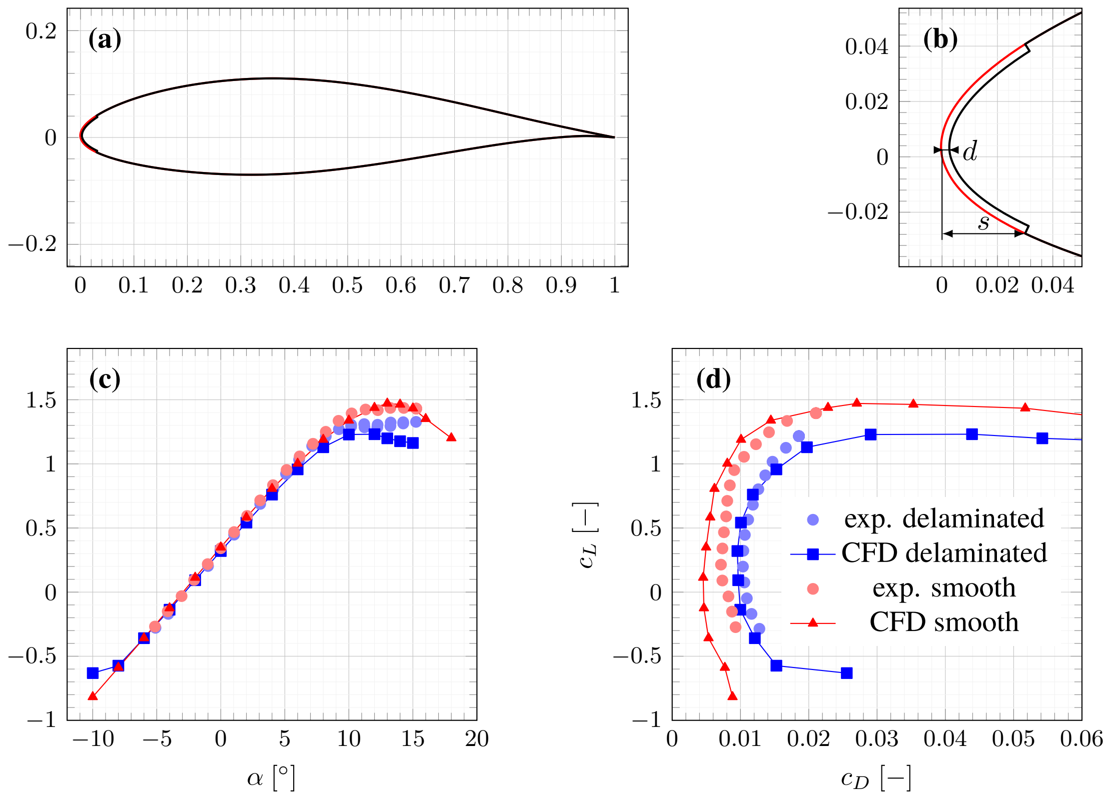

Fig. 4: The delaminated model on the NACA 64_3-618 geometry is shown in the subfigures (a) and (b). The numerically estimated lift and polar curves for airfoils with and without delamination damage are compared to experimental data [7] for a Reynolds number of $5 \cdot 10^6$ in the subfigures (c) and (d).

4. Conclusions

Wind turbine blades are constantly exposed to different weather conditions. Particularly, airborne particles, droplets, or insects might impact the leading edge with high relative velocities and erode the surface. The computations of the Navier-Stokes equations can accurately predict flow separation and losses, given that the surface roughness is correctly modelled. Therefore, the impact of the surface roughness on the aerodynamic performance was simulated using a mathematical description and a geometrically resolved procedure. The simulation strategies have been validated against data from the literature for two-dimensional airfoils, revealing satisfying agreement. More details on this work can be found in Holzinger [5].

References

[1] B Amirzadeh et al. “A computational framework for the analysis of rain-induced erosion in wind turbine blades, part I: Stochastic rain texture model and drop impact simulations”. In: *Journal of Wind Engineering and Industrial Aerodynamics* 163 (2017), pp. 33–43.

[2] María Isabel Blanco. “The economics of wind energy”. In: *Renewable and sustainable energy reviews* 13.6-7 (2009), pp. 1372–1382.

[3] A Castorrini et al. “Assessing wind turbine energy losses due to blade leading edge erosion cavities with parametric CAD and 3D CFD”. In: *Journal of Physics: Conference Series*. Vol. 1618. 5. IOP Publishing. 2020, p. 052015.

[4] Woobeom Han, Jonghwa Kim, and Bumsuk Kim. “Effects of contamination and erosion at the leading edge of blade tip airfoils on the annual energy production of wind turbines”. In: *Renewable energy* 115 (2018), pp. 817–823.

[5] Christoph Holzinger. “Leading Edge Erosion: A Review and Application of Modeling Strategies for the Investigation of Erosion-induced Effects on Wind Turbine Rotor Blades”. MA thesis. TU Wien, 2022.

[6] Mark Hugh Keegan, DH Nash, and MM Stack. “On erosion issues associated with the leading edge of wind turbine blades”. In: *Journal of Physics D: Applied Physics* 46.38 (2013), p. 383001.

[7] Emil Krog Kruse, Christian Bak, and Anders Smærup Olsen. “Wind tunnel experiments on a NACA 633-418 airfoil with different types of leading edge roughness”. In: *Wind Energy* 24.11 (2021), pp. 1263–1274.

[8] Christopher M. Langel et al. “RANS Based Methodology for Predicting the Influence of Leading Edge Erosion on Airfoil Performance”. In: *Sandia National Laboratories* SAND2017-11289 (2017).

[9] Robin B Langtry and Florian R Menter. “Correlation-based transition modeling for unstructured parallelized computational fluid dynamics codes”. In: *AIAA journal* 47.12 (2009), pp. 2894–2906.

[10] Hamish Law and Vasileios Koutsos. “Leading edge erosion of wind turbines: Effect of solid airborne particles and rain on operational wind farms”. In: *Wind Energy* 23.10 (2020), pp. 1955–1965.

[11] Florian R Menter. “Two-equation eddy-viscosity turbulence models for engineering applications”. In: *AIAA journal* 32.8 (1994), pp. 1598–1605.

[12] Kieran Pugh, Ghulam Rasool, and Margaret M Stack. “Some thoughts on mapping tribological issues of wind turbine blades due to effects of onshore and offshore raindrop erosion”. In: *Journal of Bio-and Tribo-Corrosion* 4 (2018), pp. 1–8.

[13] Matthias Schramm et al. “The influence of eroded blades on wind turbine performance using numerical simulations”. In: *Energies* 10.9 (2017), p. 1420.

[14] W Timmer. “An overview of NACA 6-digit airfoil series characteristics with reference to airfoils for large wind turbine blades”. In: *47th AIAA aerospace sciences meeting including the new horizons forum and aerospace exposition*. Vol. AIAA 2009-268. 2009, pp. 1–13.

[15] Yan Wang, Ruifeng Hu, and Xiaojing Zheng. “Aerodynamic analysis of an airfoil with leading edge pitting erosion”. In: *Journal of Solar Energy Engineering* 139.6 (2017), p. 061002.